Identification of the Proton Pathway in Bacterial Reaction Centers: Cooperation between Asp-M17 and Asp-L210 Facilitates Proton Transfer to the Secondary Quinone (Q_B)†

M. L. Paddock, P. Ädelroth, C. Chang, E. C. Abresch, G. Feher, and M. Y. Okamura*

Department of Physics 0319, 9500 Gilman Drive, University of California, San Diego, La Jolla, California 92093

Received February 8, 2001

ABSTRACT: The reaction center (RC) from *Rhodobacter sphaeroides* uses light energy to reduce and protonate a quinone molecule, Q_B (the secondary quinone electron acceptor), to form quinol, Q_BH_2. Asp-L210 and Asp-M17 have been proposed to be components of the pathway for proton transfer [Axelrod, H. L., Abresch, E. C., Paddock, M. L., Okamura, M. Y., and Feher, G. (2000) *Proc. Natl. Acad. Sci. U.S.A. 97*, 1542−1547]. To test the importance of these residues for efficient proton transfer, the rates of the proton-coupled electron-transfer reaction $k_{AB}^{(2)}$ ($Q_A^{-\bullet}Q_B^{-\bullet} + H^+ \rightleftarrows Q_A^{-\bullet}Q_BH^\bullet \rightarrow Q_AQ_BH^-$) and its associated proton uptake were measured in native and mutant RCs, lacking one or both Asp residues. In the double mutant RCs, the $k_{AB}^{(2)}$ reaction and its associated proton uptake were ∼300-fold slower than in native RCs (pH 8). In contrast, single mutant RCs displayed reaction rates that were ≤3-fold slower than native (pH 8). In addition, the rate-limiting step of $k_{AB}^{(2)}$ was changed from electron transfer (native and single mutants) to proton transfer (double mutant) as shown from the lack of a dependence of the observed rate on the driving force for electron transfer in the double mutant RCs compared to the native or single mutants. This implies that the rate of the proton-transfer step was reduced ($\geq 10^3$-fold) upon replacement of both Asp-L210 and Asp-M17 with Asn. Similar, but less drastic, differences were observed for $k_{AB}^{(1)}$, which at pH ≥8 is coupled to the protonation of Glu-L212 [$(Q_A^{-\bullet}Q_B)$—$Glu^- + H^+ \rightarrow (Q_AQ_B^{-\bullet})$—GluH]. These results show that the pathway for proton transfer from solution to reduced Q_B involves both Asp-L210 and Asp-M17, which provide parallel branches to the proton-transfer pathway and through their electrostatic interaction have a cooperative effect on the proton-transfer rate. A possible mechanism for the cooperativity is discussed.

The conversion of light into chemical energy in photosynthetic bacteria is initiated within a membrane-bound pigment−protein complex called the reaction center (RC).[1] The isolated RC from *Rhodobacter (Rb.) sphaeroides* is composed of three polypeptide subunits (L, M, and H), four bacteriochlorophylls, two bacteriopheophytins, one internally bound non-heme-Fe^{2+}, and two ubiquinone (UQ_{10}) molecules (reviewed in *1* and *2*). Light induces electron transfer from the primary donor (a bacteriochlorophyll dimer) through a series of acceptor molecules (a bacteriopheophytin and a quinone molecule, Q_A) to a loosely bound secondary quinone, Q_B. Q_B accepts two electrons, sequentially transferred through the electron-transfer chain, and two protons [labeled $H^+(1)$ and $H^+(2)$, respectively],[2] through the proton-transfer pathways, to form quinol Q_BH_2.

The first electron transfer to Q_B [$k_{AB}^{(1)}$] does not involve direct protonation of the quinone (eq 1), but at pH ≥8 is coupled to the protonation of Glu-L212. This step involves the uptake of $H^+(2)$, which is transferred to reduced Q_B following the second electron reduction (eqs 2 and 3).

$$(Q_A^{-\bullet}Q_B)\text{—}Glu^- + H^+(2) \xrightarrow{k_{AB}^{(1)}} (Q_AQ_B^{-\bullet})\text{—}GluH \quad (1)$$

The second electron transfer [$k_{AB}^{(2)}$] is coupled to the first direct protonation of the semiquinone and involves the uptake of $H^+(1)$ (eq 2). The mechanism of the proton-coupled electron-transfer reaction $k_{AB}^{(2)}$ (eq 2) was shown to be a two-step process in which fast protonation precedes rate-limiting electron transfer (*3*).

$$Q_A^{-\bullet}Q_B^{-\bullet} + H^+(1) \overset{\text{fast}}{\rightleftharpoons} Q_A^{-\bullet}Q_BH^\bullet \xrightarrow{\text{slow}} Q_AQ_BH^- \quad (2)$$

† This work was supported by the National Science Foundation (NSF Grant MCB94-16652) and National Institutes of Health (NIH Grants GM 41637 and GM 13191) and by a postdoctoral fellowship from the Swedish Foundation for International Cooperation in Research and Higher Education (STINT) to P.Ä.

* Address correspondence to this author at the Department of Physics 0319, 9500 Gilman Dr., University of California, San Diego, La Jolla, CA 92093. Phone: (858) 534-2505, Fax: (858) 822-0007, E-mail: mokamura@ucsd.edu.

[1] Abbreviations: D, primary donor; Q_A, primary quinone electron acceptor; Q_B, secondary quinone electron acceptor; RC, reaction center; cyt *c*, horse heart cytochrome *c*.

[2] The nomenclature $H^+(1)$ and $H^+(2)$ refers to the sequence of protonation of reduced Q_B and not to the sequence of proton uptake associated with the first and second flash excitations. Thus, upon flash excitation, $H^+(2)$ is taken up before $H^+(1)$, but protonates Glu-L212 and not reduced Q_B. It is subsequently transferred following the second electron transfer to protonate $Q_BH^-(1)$ (eq 3).

10.1021/bi010280a CCC: $20.00
Published on Web 05/16/2001

Subsequent internal proton transfer of $H^+(2)$ from Glu-L212 (eq 3) leads to the formation of quinol.

$$(Q_AQ_BH^-)—GluH \rightarrow (Q_AQ_BH_2)—Glu^- \qquad (3)$$

Note that $H^+(2)$ is taken up from solution during the first electron-transfer step (eq 1), but does not bind to reduced Q_B until after the second electron-transfer step (eq 3). The fully reduced quinol, Q_BH_2, serves as a mobile electron and proton carrier (*4*−*6*), transferring electrons and protons from the RC to the cytochrome bc_1 complex (eq 2). Binding of neutral quinone from an exogenous pool resets the system for repeated photochemistry.

In the membrane-bound RC, the protons involved in the reactions described by eqs 1−3 are taken up from the cytoplasm. Parts of the pathways for these proton-transfer events have been determined from studies of the effects of site-directed mutations in isolated RCs (*7*−*12*). Three residues (Glu-L212, Ser-L223, and Asp-L213), located near $Q_B^{-\bullet}$ (≤5 Å), were shown to be crucial (reviewed in *13*). The entry point of the protons was identified to be near His-H126, His-H128, and Asp-H124, the binding position of the proton-transfer inhibitors Zn^{2+} and Cd^{2+} (*14*, *15*).

The importance of Asp-L210 and Asp-M17, located between the entry point and $Q_B^{-\bullet}$, was deduced from the results of measurements made on RCs with a bound Cd^{2+} (*16*). In these RCs, the proton-transfer step of eq 2 becomes rate-limiting. In Cd^{2+}-RCs with either Asp-L210 or Asp-M17 replaced with Asn, the observed rate of proton transfer was decreased ∼10-fold (*16*).

In this study, we investigated the importance of Asp-L210 and Asp-M17 for proton transfer to reduced Q_B through the physiological proton-transfer pathway, i.e., in the absence of a bound metal ion. We measured the proton-coupled electron transfers $k_{AB}^{(1)}$ (eq 1) and $k_{AB}^{(2)}$ (eq 2) to determine the effect of mutation on the rate of proton transfer and k_{BD} ($D^+Q_AQ_B^{-\bullet} \rightarrow DQ_AQ_B$) to probe the effect of the mutations on the electrostatic environment near $Q_B^{-\bullet}$. In addition, we measured proton uptake from solution and compared its rate to $k_{AB}^{(1)}$ and $k_{AB}^{(2)}$. We assessed changes in the above-mentioned reactions in two single mutant RCs, DN(L210) [Asp-L210 → Asn] and DN(M17) [Asp-M17 → Asn], the double mutant DN(L210)/DN(M17) [Asp-L210 → Asn/Asp-M17 → Asn], and the triple mutant DN(L210)/DN(M17)/EQ(L212) [Asp-L210 → Asn/Asp-M17 → Asn/Glu-L212 → Gln]. A preliminary account of this work has been presented (*17*).

MATERIALS AND METHODS

Reagents and Quinones. Q_{10} (coenzyme Q_{10}; 2,3-dimethoxy-5-methyl-6-decaisoprenyl-1,4-benzoquinone) and MQ_4 (menatetrenone; 2-methyl-3-tetraisoprenyl-1,4-naphthoquinone) were obtained from Sigma. Me_3NQ (2,3,5-trimethyl-1,4-naphthoquinone) and Me_4NQ (2,3,6,7-tetramethyl-1,4-naphthoquinone) were kindly provided by J. M. Bruce, University of Manchester, Manchester, U.K. The Q_B site inhibitor stigmatellin (prepared in ethanol) was obtained from Fluka. Horse heart cytochrome *c* (cyt *c*) was obtained from Sigma, reduced (>95%) by hydrogen gas on platinum black (Aldrich), and filtered (0.2 μm pore size acetate filter). Synthetic oligonucleotides were obtained from IDT DNA (Coralville, IA). All other reagents were of analytical grade.

Site-Directed Mutagenesis. The site-directed mutations Asp-L210 → Asn [DN(L210)] and Asp-M17 → Asn [DN(M17)] were constructed as previously described (*7*). The double mutation of Asp-L210 → Asn/Asp-M17 → Asn [DN(L210)/DN(M17)] was constructed in two sequential steps using the QuikChange Mutagenesis kit (Stratagene) and a Perkin-Elmer PCR System. First, the Asp-L210 → Asn mutation was introduced into a pBC plasmid (Stratagene) carrying most of *puf L* and all of *puf M* [from the *Asp-718* site to the *Hin*dIII site (*18*)]. Following polymerization and transformation, colonies were isolated, and DNA was purified using QiaPrep Miniprep (Qiagen) and sequenced (MacConnell Research Corp., San Diego, CA) to identify clones with only the desired mutation. The single mutant plasmid was then used as the template for incorporation of the Asp-M17 → Asn mutation using the QuikChange Mutagenesis kit. The triple mutation of Asp-L210 → Asn/Asp-M17 → Asn/Glu-L212 → Gln [DN(L210)/DN(M17)/EQ(L212)] was constructed by introducing the Glu-L212 → Gln replacement in the double mutant described above using the QuikChange Mutagenesis kit.

Isolation and Preparation of Reaction Centers. The bacteria harboring the modified RC genes were grown in the dark as described (*7*). RCs from *Rb. sphaeroides* R26 and the mutant strains were isolated in 15 mM Tris-HCl, pH 8, 0.025% lauryldimethylamine *N*-oxide (LDAO), 0.1 mM EDTA following published procedures (*19*). The final ratio of absorbance, A^{280}/A^{800}, was ≤1.3. Reconstitution of the Q_B site was achieved by incubating the RC solution with Q_{10} (∼5 Q_{10} per RC) solubilized in 1% LDAO followed by dialysis against TL buffer (10 mM Tris-HCl, pH 8.0, 0.025% lauryldimethylamine *N*-oxide). Occupancy of the Q_B sites was 80−90%. For the pH dependence studies, the RC samples were further dialyzed for 2 days against HM [10 mM Hepes, pH 7.5, 0.04% dodecyl-β-D-maltoside (Anatrace)]. Incorporation of naphthoquinones (NQ) was accomplished as described in (*3*) as modified in (*20*).

Determination of Electron- and Proton-Transfer Kinetics by Transient Optical Spectroscopy. Charge recombination rates were measured by monitoring the recovery of the donor band at 865 nm following bleaching with a single flash from an Nd:YAG laser (Opotek, Carlsbad, CA) using a single-beam spectrophotometer (*21*). All measurements were performed at 21 °C. To determine the recombination rate, k_{BD} ($D^+Q_AQ_B^{-\bullet} \rightarrow DQ_AQ_B$), the observed absorption recoveries were fitted to two exponentials using procedures previously described (*22*). The recombination rate, k_{AD} ($D^+Q_A^{-\bullet} \rightarrow DQ_A$), was measured in the presence of 10 μM stigmatellin, which blocks electron transfer to Q_B.

The rate constant, $k_{AB}^{(1)}$, for the transfer of the first electron to Q_B (eq 1) was measured by monitoring the bacteriopheophytin bandshift at 750 nm, which is differentially sensitive to the reduction state of the quinones Q_A and Q_B (*21*, *23*). To improve the signal-to-noise ratios, typically 9−36 traces were averaged.

The proton-coupled electron-transfer $k_{AB}^{(2)}$ (eq 2) was determined by monitoring the decay of the semiquinone absorption at 450 nm following a second saturating laser flash in the presence of an external reductant (20 μM horse heart cyt *c*) (*24*). The kinetic decay was fitted to a single exponential.

Table 1: Measured Rate Constants for Native and Mutant RCs (pH 8, $T = 21$ °C)[a]

RCs	first flash: electron transfer, $k_{AB}^{(1)}$ (s^{-1})[b]	first flash: proton uptake, $k_H^{(1)obs}$ (s^{-1})	second flash: electron transfer, $k_{AB}^{(2)}$ (s^{-1})	second flash: proton uptake, $k_H^{(2)obs}$ (s^{-1})	k_{AD} (s^{-1})	k_{BD} (s^{-1})
native	6×10^3	6×10^3	1×10^3	1×10^3	8.8	0.8
DN(M17)	8×10^2	8×10^2	6×10^2	6×10^2	9.0	0.7
DN(L210)	7×10^2	7×10^2	5×10^2	5×10^2	8.9	0.6
DN(L210)/DN(M17)	9×10^1	9×10^1	4	4	8.8	0.5

[a] The variation in rates in different samples was estimated to be ~20% for $k_{AB}^{(1)}$, $k_H^{(1)obs}$, $k_{AB}^{(2)}$, and $k_H^{(2)obs}$ and ~10% for k_{AD} and k_{BD}. For a comparison of k_{AB} and k_H^{obs}, the same sample was used; in this case, the reproducibility was ~5%. [b] The observed rate constant was obtained using a single-exponential fit to the data. A better fit can be obtained with a sum of two exponentials (*24*), but we opted for the simple analysis, which shows all the salient features of the mutations.

The kinetic decay in samples in which Q_{10} was replaced with NQ in the Q_A site was biexponential—one exponential was the same as measured in the unsubstituted sample due to the fraction of RCs that retained Q10 in the Q_A site, and the other exponential was due to NQ containing RCs (*3*).

Proton uptake was measured by monitoring the absorbance change of a pH-sensitive dye (40 μM *m*-cresol purple) at 580 nm in a weakly buffered RC sample as described by Ädelroth et al. (*25*).

The pH profiles of the reaction rates were measured in RC samples that were diluted into a cocktail of buffers consisting of a 5 mM aliquot of each of the following buffers: citric acid (Calbiochem), Mes [2-(*N*-morpholino)-ethanesulfonic acid, Calbiochem], Pipes (1,4-piperazinediethanesulfonic acid, Calbiochem), Tris [2-amino-2-(hydroxymethyl)propane-1,3-diol, Fisher], Ches (cyclohexylaminoethanesulfonic acid, Calbiochem), and Caps [3-(cyclohexylamino)-1-propanesulfonic acid, Calbiochem]. The pH of the solution was adjusted by adding either 1 N HCl or 1 N NaOH. pH measurements were performed with a Cole-Palmer Chemcadet pH meter equipped with a Toledo-Mettler U402-M3 pH electrode and calibrated with standards, which spanned the measured pH values. The uncertainty in reported pH values was ±0.05 unit.

RESULTS

The First Electron-Transfer Rate, $k_{AB}^{(1)}$ (eq 1), and Associated Proton Uptake, $k_H^{(1)obs}$. The transfer rates for the first electron to Q_B [$k_{AB}^{(1)}$, eq 1], measured at 750 nm, were reduced ~8-fold in the DN(M17) and DN(L210) mutants compared to native RCs at pH 8 (Table 1). A greater decrease was observed in the double mutant [DN(L210)/DN(M17)] RCs, in which $k_{AB}^{(1)}$ was decreased ~70-fold compared to native RCs at pH 8 (Figure 1A). In contrast, a more native-like value was observed in the triple mutant [DN(L210)/DN(M17)/EQ(L212)] RCs (~3-fold smaller than in native).

Associated with the formation of $D^+Q_B^{-\bullet}$, the rates of proton uptake [$k_H^{(1)obs}$] were 6000 s^{-1} for native RCs and 90 s^{-1} for the double mutant RCs (Figure 1B). These rates correspond to the rate of electron transfer, $k_{AB}^{(1)}$. In the triple mutant, which contains the additional Glu-L212 → Gln mutation, the amplitude of proton uptake at pH 8.0 was significantly decreased by an order of magnitude from that observed in the double mutant (data not shown).

The pH dependence of $k_{AB}^{(1)}$ in native RCs displays a classic pH titration with a pK_a ~ 8.5 with the observed rate decreasing with increasing pH (Figure 2); i.e., $k_{AB}^{(1)}$ is constant when pH ≪9 and decreases 10-fold per pH unit when pH ≫9. In both of the single mutant RCs, $k_{AB}^{(1)}$ at pH <6 is essentially the same as in native RCs. However, the pH dependence is shifted to lower pH by ~2 pH units. In contrast, the pH dependence of $k_{AB}^{(1)}$ for the double mutant no longer resembles a classic titration, but shows a linear dependence of $k_{AB}^{(1)}$ that is proportional to $[H^+]^{0.7}$ (Figure 2); i.e., $k_{AB}^{(1)}$ decreases 5-fold per pH unit.

In the triple mutant RCs [DN(L210)/DN(M17)/EQ(L212)], no pH dependence of $k_{AB}^{(1)}$ was observed (data not shown). Thus, the additional introduction of the Glu-L212 → Gln mutation results in the removal of the pH titration, as has been observed before in the single Glu-L212 → Gln mutant RCs (*7*−*9*).

The Proton-Coupled Electron-Transfer Rate, $k_{AB}^{(2)}$ (eq 2), and Associated Proton Uptake, $k_H^{(2)obs}$. The rate of transfer of the second electron to Q_B [$k_{AB}^{(2)}$, eq 2], following a second saturating laser flash, was measured at 450 nm in native RCs to be 1100 s^{-1} at pH 8 (Table 1). In the DN(M17) and DN(L210) RCs, $k_{AB}^{(2)}$ was not greatly affected, being decreased less than 3-fold from the native value (Table 1). In contrast, $k_{AB}^{(2)}$ in the DN(L210)/DN(M17) double mutant RCs was ~300-fold smaller than the native value (Figure 3A).

Proton uptake coupled with the formation of $DQ_AQ_BH_2$ (eq 2) was measured in isolated RCs using the pH-sensitive dye *m*-cresol purple. The observed rate of proton uptake [$k_H^{(2)obs}$] was found to be decreased ~300-fold to 4 s^{-1} in the double mutant compared to native RCs (Figure 3B). The observed proton uptake rate constants were the same as $k_{AB}^{(2)}$ measured in Figure 3A (Table 1).

The pH profile of $k_{AB}^{(2)}$ in native RCs shows two distinct regions. Below pH ~8, $k_{AB}^{(2)}$ decreases with increasing pH, with $k_{AB}^{(2)}$ proportional to $[H^+]^{0.4}$ (Figure 4). Above pH ~8, the decrease with increasing pH becomes more pronounced, with $k_{AB}^{(2)}$ proportional to $[H^+]^1$. A similar pH dependence of $k_{AB}^{(2)}$ is observed in the DN(L210) and DN(M17) mutant RCs with a shift of ≤0.5 pH unit to lower pH (Figure 4). In contrast, the double [DN(L210)/DN(M17)] mutant RCs displayed a modified pH dependence with $k_{AB}^{(2)}$ proportional to $[H^+]^{0.7}$ throughout the entire pH range from 5 to 9 (Figure 4). Above pH >9, $k_{AB}^{(2)}$ becomes difficult to measure due to the unfavorable transfer of the first electron to Q_B (see k_{BD} below).

The dependence of $k_{AB}^{(2)}$ on the driving force for electron transfer was measured as described by Graige et al. (*3*), by replacing the native Q_{10} in the Q_A site with a series of naphthoquinones. As previously reported, $k_{AB}^{(2)}$ in the native and single mutant, DN(L210) and DN(M17), RCs was dependent on the driving force for electron transfer (*16*),

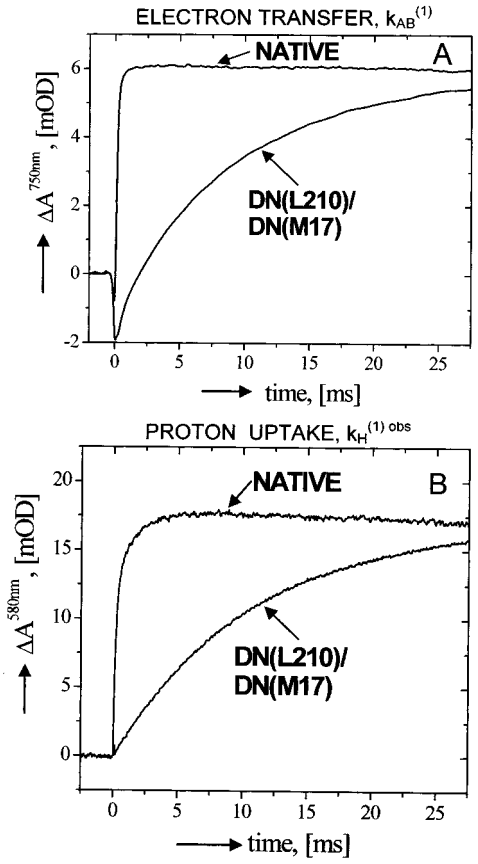

FIGURE 1: Absorbance changes at 750 nm (A) and at 580 nm (B) as a function of time following a saturating laser flash in the native and DN(L210)/DN(M17) [Asp-L210 → Asn/Asp-M17 → Asn] double mutant RCs. The kinetics are due to the proton-coupled electron-transfer reaction $k_{AB}^{(1)}[(Q_A^{-\bullet}Q_B)—Glu^- + H^+ \rightarrow (Q_AQ_B^{-\bullet})—GluH]$ (eq 1). (A) The absorbance at 750 nm is sensitive to the reduction states of the quinones Q_A and Q_B (*21*, *23*). The absorbance decrease immediately after the laser flash is due to a decreased absorption upon the rapid formation of the $D^+Q_A^{-\bullet}$ state, which differs slightly between native and the double mutant RCs. From a fit of the kinetics to an exponential function, the rate constant $k_{AB}^{(1)}$ was determined; the native kinetic decay is not resolvable on this time scale. The kinetic rise in the double mutant is ~70-fold slower than in native RCs (Table 1). The single mutant RCs [DN(L210) and DN(M17)] show an ~8-fold slower kinetic rise than native RCs (not shown) (Table 1). (Conditions: 2 μM RCs in HM buffer, pH 8; average of 200 traces.) (B) The absorbance rise at 580 nm is due to a change in absorption of the pH-sensitive dye *m*-cresol purple caused by proton uptake coupled with the quinone reduction. Traces represent the differences between traces obtained in unbuffered solution and traces obtained after addition of 5 mM Tris. From the absorbance changes, the proton uptake rate was obtained. This rate is the same as $k_{AB}^{(1)}$, as determined in (A). The amplitude of the proton uptake at pH 8 in the double mutant RCs was 0.7 H^+/RC, compared to 0.35 H^+/RC in native RCs. This amplitude increase is attributed to the lower pK_a of Glu-L212 in the double mutant than in native RCs. Analogous changes in the proton uptake by Glu-L212 are observed in the FTIR spectra (*26*). The absorbance changes correspond to native RCs; the amplitudes of the mutant RCs have been normalized (decreased ~2-fold) to better illustrate the change in the rate. (Conditions: 2 μM RCs, 25 mM KCl, 0.04% β-D-maltoside, 40 μM m-cresol purple, pH 8; average of 10 traces.)

increasing ~7-fold in RCs containing Me_3NQ in the Q_A site (Figure 5). In contrast, $k_{AB}^{(2)}$ in the DN(L210)/DN(M17) double mutant RCs did not depend on the electron driving force (Figure 5), showing that the mechanism of the reaction had changed.

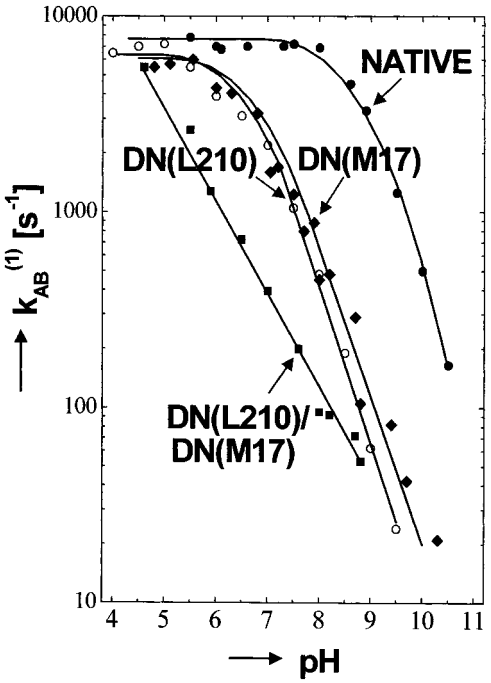

FIGURE 2: pH dependence of $k_{AB}^{(1)}$ for native (●) and mutant DN(M17) [Asp-M17 → Asn] (◆), DN(L210) [Asp-L210 → Asn] (○), and DN(L210)/DN(M17) [Asp-L210 → Asn/Asp-M17 → Asn] (■) RCs. The pH dependence in native RCs displays a simple pH titration with a pK_a ~ 9. In both of the single mutant RCs, the saturating level at pH <6 is essentially unchanged from the $k_{AB}^{(1)}$ value observed in the native RCs, but the pH titration is shifted to lower pH by ~2 pH units. In contrast, the pH dependence of $k_{AB}^{(1)}$ for the DN(L210)/DN(M17) double mutant no longer resembles a simple titration, but shows a linear dependence proportional to $[H^+]^{0.7}$. (Conditions: same as in Figure 1 with a mixture of buffers (see Materials and Methods).]

The Charge Recombination Rates, k_{AD} and k_{BD}. The charge recombination rates for the reactions $D^+Q_A^{-\bullet} \rightarrow DQ_A$ (k_{AD}) and $D^+Q_AQ_B^{-\bullet} \rightarrow DQ_AQ_B$ (k_{BD}) were measured at 865 nm. At pH 8, the measured values of k_{AD} (~9 s^{-1}) and k_{BD} (~1 s^{-1}) were approximately the same for native, the single mutants DN(M17) [Asp-M17 → Asn] and DN(L210) [Asp-L210 → Asn], the double mutant DN(L210)/DN(M17) [Asp-L210 → Asn/Asp-M17 → Asn], and the triple mutant DN(L210)/DN(M17)/EQ(L212) [Asp-L210 → Asn/Asp-M17 → Asn/Glu-L212 → Gln] (Table 1).

The pH dependence of k_{AD} is very weak, ranging from ~6 s^{-1} at pH 5 to ~11 s^{-1} at pH 11 in all of the samples (data not shown). In contrast, k_{BD} shows a greater change as the pH is changed in native RCs, increasing from ~0.2 s^{-1} at pH 5 to ~3 s^{-1} at pH 11.

In native RCs, two apparent titrations of k_{BD} are observed, one below pH 7 and another above pH 8 (data not shown). Both single and double mutant RCs displayed pH profiles for k_{BD} similar to each other with nearly the same plateau value at low pH and an increase in value above pH ~8. Thus, the double mutant RCs show no significant difference in $Q_B^{-\bullet}$ stability compared to either single mutant. The pH profiles measured in the mutant RCs differ most from that of native in that the higher pH titration is slightly shifted to lower pH (<1 pH unit) and the low pH titration is shifted out of the experimental pH range (i.e., it is shifted below pH 4.5 and is absent in two of the mutant samples).

Unlike the other RCs, the triple mutant RCs [DN(L210)/DN(M17)/EQ(L212)] show no dependence of k_{BD} on pH

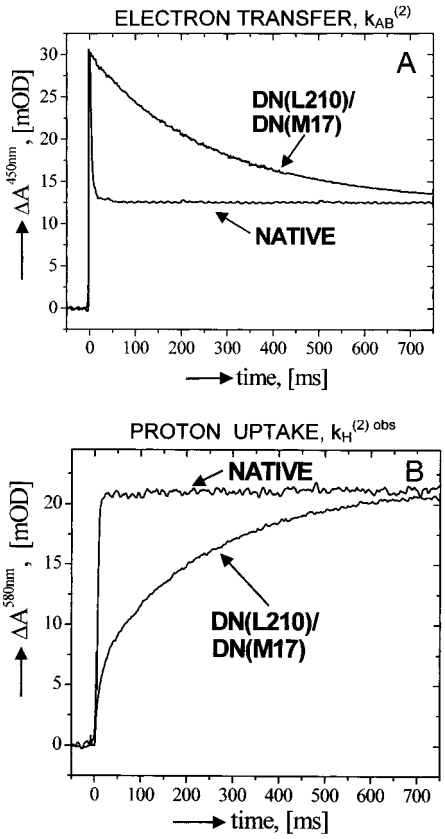

FIGURE 3: Absorbance decay of the semiquinones at 450 nm (A) and absorbance increase of the pH-sensitive dye *m*-cresol purple at 580 nm (B) as a function of time following the second laser flash in native and DN(L210)/DN(M17) [Asp-L210 → Asn/Asp-M17 → Asn] double mutant RCs. The transients are associated with the second reduction of Q_B, i.e., $Q_A^{-\bullet}Q_B^{-\bullet} + H^+ \rightleftarrows Q_A^{-\bullet}Q_BH^\bullet \rightarrow Q_AQ_BH^-$ (eq 2). (A) From the kinetic decay, the rate constant $k_{AB}^{(2)}$ was determined. Note the ~300-fold slower kinetic decay [$1/k_{AB}^{(2)} \cong 250$ ms] in the double mutant. The single DN(L210) [Asp-L210 → Asn] and DN(M17) [Asp-M17 → Asn] RCs (data not shown) displayed kinetics that were only slightly different from native (<3-fold slower) and not resolvable from the native kinetic trace on this time scale. The pedestal at long times is due to the absorbance change of cyt *c* used to reduce the primary donor (see Materials and Methods). (Conditions: 2 μM RCs in HM buffer pH 8.) (B) The absorbance rise at 580 nm is due to a change in absorption of the pH-sensitive dye *m*-cresol purple caused by proton uptake coupled with the quinone reduction. Traces represent the differences between traces obtained in unbuffered solution and traces obtained after addition of 5 mM Tris. From the absorbance changes, the proton uptake rate was obtained. This rate is the same as $k_{AB}^{(2)}$, as determined in (A). The absorbance changes correspond to native RCs; the amplitudes of the mutant RCs have been normalized (increased ~50%) to better illustrate the change in the rate. (Conditions: 2 μM RCs, 25 mM KCl, 0.04% β-D-maltoside, 20 μM cyt *c*, 40 μM m-cresol purple, pH 8.)

(data not shown). Thus, the additional introduction of the Glu-L212 → Gln mutation results in the removal of the higher pH titration, as has been observed before in the single Glu-L212 → Gln mutant RCs (*7*−*9*).

DISCUSSION

The goal of this study was to elucidate the pathway for proton transfer from solution to the bound semiquinone $Q_B^{-\bullet}$ in isolated RCs from *Rb. sphaeroides* by measuring the effects of mutations on the rate of proton transfer. A difficulty that had to be overcome is the fact that proton transfer in native RCs is not the rate-limiting step for the measured reactions, and, therefore, changes of the rate of proton transfer may have no effect on the observed rates. To obtain information about the rate of proton transfer, conditions have to be established under which proton transfer becomes rate-limiting. This had been previously accomplished in RCs having a bound Cd^{2+} (*16*). The replacement of Asp-L210 or

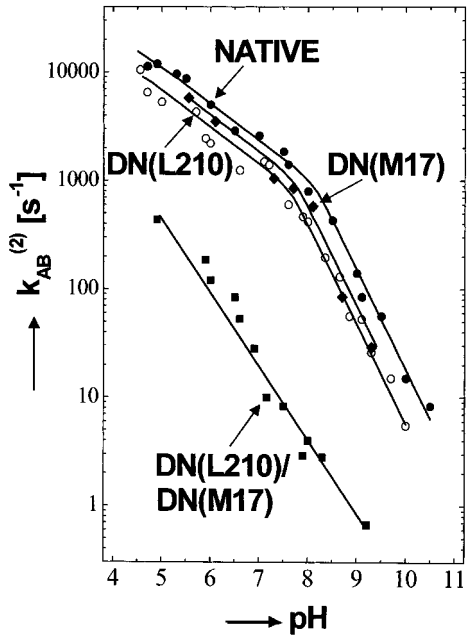

FIGURE 4: pH dependence of $k_{AB}^{(2)}$ for native (●) and mutant DN(M17) [Asp-M17 → Asn] (◆), DN(L210) [Asp-L210 → Asn] (○), and DN(L210)/DN(M17) [Asp-L210 → Asn/Asp-M17 → Asn] (■) RCs. In native RCs, $k_{AB}^{(2)}$ is proportional to $[H^+]^{0.4}$ for pH <8 and to $[H^+]^1$ for pH >8. The pH dependences observed for the DN(L210) and DN(M17) mutant RCs are similar to each other with a shift of ≤0.5 pH unit to lower pH compared to native RCs. In contrast, the DN(L210)/DN(M17) mutant RCs displayed a modified pH dependence with $k_{AB}^{(2)}$ proportional to $[H^+]^{0.7}$ throughout the entire pH range from 5 to 9. [Conditions: same as in Figure 3 with a mixture of buffers (see Materials and Methods).]

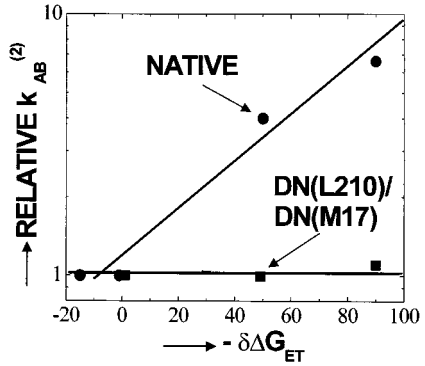

FIGURE 5: Driving force dependence of $k_{AB}^{(2)}$ in native and DN(L210)/DN(M17) [Asp-L210 → Asn/Asp-M17 → Asn] (■) double mutant RCs. The driving force for electron transfer was changed by replacing the native Q_{10} (defined to be at $\delta\Delta G_{ET} = 0$ meV) in the Q_A site with several naphthoquinones: MQ_4 ($\delta\Delta G_{ET} = -50$ meV) and Me_3NQ ($\delta\Delta G_{ET} = -90$ meV). As previously reported, $k_{AB}^{(2)}$ in native RCs was dependent on the driving force for electron transfer (*3*). In contrast, the DN(L210)/DN(M17) double mutant RCs displayed no dependence of $k_{AB}^{(2)}$ on the electron driving force, showing that the mechanism of the reaction has changed. The DN(L210) and DN(M17) single mutant RCs showed driving force dependence similar to native RCs (data not shown) (*16*). (Conditions same as in Figure 3.)

Asp-M17 with Asn in the Cd^{2+}-bound RCs decreased the observed rate of proton transfer ~10-fold, showing the importance of these residues in facilitating proton transfer. In the present work, we investigate the importance of Asp-L210 and Asp-M17 in the absence of a Cd^{2+} ion through the construction of a double mutant in which both Asp-L210 and Asp-M17 were replaced with Asn, which makes proton transfer the rate-limiting step.

The effects of the single and double mutations on the coupled electron-transfer reactions $k_{AB}^{(1)}$ [$(Q_A^{-\bullet}Q_B)$—$Glu^- + H^+ \rightarrow (Q_AQ_B^{-\bullet})$—GluH] (eq 1) and $k_{AB}^{(2)}$ [$Q_A^{-\bullet}Q_B^{-\bullet} + H^+ \rightarrow Q_A(Q_BH)^-$] (eq 2) and on proton uptake from solution were determined and used to delineate the proton-transfer pathways as discussed below.

Simultaneous Replacement of Asp-L210 and Asp-M17 with Asn Decreases the Rate of Proton Uptake.

(A) Uptake of the First Proton [$H^+(1)$] during $k_{AB}^{(2)}$. The most striking result of this study is the observation that the double replacement of Asp-L210 and Asp-M17 with Asn decreases $k_{AB}^{(2)}$ and $k_H^{(2)obs}$ from ~1200 to ~4 s^{-1} (i.e., by 300-fold at pH 8) (Figure 3) while the single mutations produce almost no changes (≤3-fold) (Table 1, Figure 4). This result is attributed to a sufficiently large change in the rate of proton transfer to make it the rate-limiting step in the double mutant RCs (see eq 2). In native RCs, the first step in eq 2 involves the fast reversible protonation of the anionic semiquinone $Q_B^{-\bullet}$. This is followed by rate-limiting electron transfer (*3*). The small effect on $k_{AB}^{(2)}$ due to the single replacements of Asp-L210 or Asp-M17 with Asn indicates that the reduction in the proton-transfer rates in these mutant RCs is not sufficient to make proton transfer the rate-limiting step. In contrast, the large effect on $k_{AB}^{(2)}$ due to the double replacement of Asp-L210 and Asp-M17 with Asn indicates that the proton-transfer step has been reduced sufficiently to become rate-limiting.

Conclusive evidence that proton transfer (step 1 in eq 2) has become rate-limiting in the double mutant comes from measurements of the dependence of $k_{AB}^{(2)}$ on the driving force for electron transfer. In native RCs and in single mutant RCs, the driving force for $k_{AB}^{(2)}$ exhibits a Marcus dependence typical of a rate-limiting electron transfer (*3, 16*). In contrast, $k_{AB}^{(2)}$ in the double mutant RCs is independent of driving force (Figure 5), indicating a change in the rate-limiting step; i.e., the proton-transfer step has become rate-limiting. These changes in driving force dependence are similar to those observed in native RCs upon binding of the proton-transfer inhibitors Zn^{2+}, Cd^{2+}, or Ni^{2+} (*14*). In analogy with the metal binding results, we conclude that the simultaneous replacement of Asp-L210 and Asp-M17 with Asn decreases the rate of proton uptake of $H^+(1)$ associated with $k_{AB}^{(2)}$ (eq 2), making proton transfer rate-limiting.

The results presented above show that the single replacement of either Asp-L210 or Asp-M17 with Asn does not block proton transfer. Since $k_{AB}^{(2)}$ increases with increasing electron-transfer driving force (Figure 5), the electron-transfer step of eq 2 remains rate-limiting. This implies that the rate of proton transfer (first step in eq 2) is faster than the observed rate [i.e., $k_{H^+} \gg k_{AB}^{(2)}$], allowing us to set a limit for $k_{H^+} \geq 10^4$ s^{-1} (pH 8). In contrast, the simultaneous replacement of both Asp with Asn (double mutant RCs) significantly reduces the proton-transfer rate, making it become the rate-limiting step of eq 2, implying that in the double mutant $k_{H^+} = k_{AB}^{(2)} = 4$ s^{-1}. Thus, the rate of proton transfer in the double mutant is decreased ≥10^3-fold.

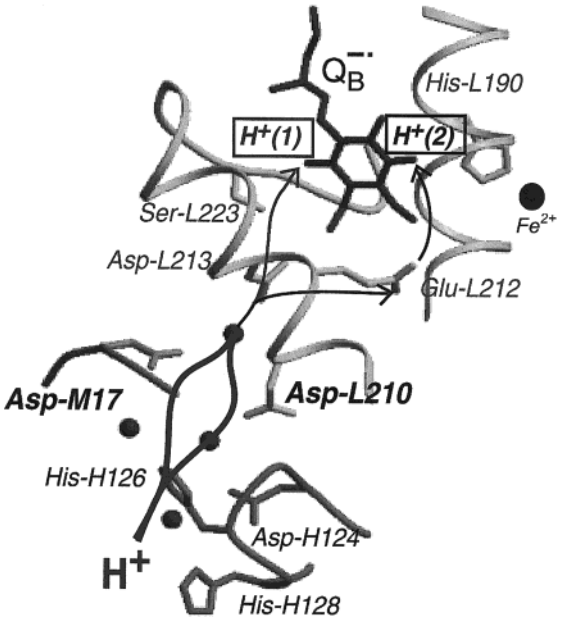

FIGURE 6: Part of the RC structure showing the region between the proton entry point and $Q_B^{-\bullet}$ (*29*). The entry point was identified by locating the binding positions of the proton-transfer inhibitors Zn^{2+}, Cd^{2+}, and Ni^{2+} (*14, 15*), which bind to Asp-H124, His-H126, and His-H128 and/or Asp-M17. Located between the entry point and $Q_B^{-\bullet}$ are Asp-L210, Asp-M17, Asp-L213, Ser-L223, and Glu-L212 (as indicated) and several water molecules (small spheres). The smooth lines represent the proton-transfer pathways for the two protons taken upon reduction of Q_B to Q_BH_2 (eqs 1−3). The kinetic results presented in this work show that Asp-L210 and Asp-M17 are involved in both proton uptake steps (heavier portion of the lines) of $H^+(1)$ to $Q_B^{-\bullet}$ (eq 2) and $H^+(2)$ to Glu-L212 (eq 1). The illustration was made using the programs MOLSCRIPT (*30*), RASTER3D (*31*), and Adobe Illustrator.

We attribute the observed changes in the proton-transfer rate to local effects of the mutations. We exclude the possibility that the mutation introduces significant long-range structural changes that propagate to the Q_B site. Long-range structural changes have been observed in second site suppressor mutations (*20, 27, 28*). In these mutant RCs, however, k_{BD} was altered. Since k_{BD} in the mutant RCs presented in this work remains essentially the same as in native RCs (Table 1), we consider such structural changes to be unlikely in the present mutant RCs. k_{BD} is also a sensitive probe of the electrostatic environment near Q_B (*7, 9, 10*). The similarity of the value and pH dependences of k_{BD} between the single and double mutant RCs implies that any significant electrostatic changes which result from the amino acid replacements are localized near the sites of mutation (Figure 6).

The reduction in the proton-transfer rate may be attributed to several possible causes: (i) the removal of the proton relay components, Asp-L210 and Asp-M17; (ii) an increase in the electrostatic barrier for bringing protons to or near L210 and M17, caused by replacing two (partially) anionic Asp residues with neutral Asn residues; (iii) possible effects on the local protein dynamics that may be important for proton delivery. The relative importance of these causes will be further investigated by (i) replacing Asp with Lys at a single site, which should lead to similar changes in the electrostatic

environment (i.e., removal of two negative charges) as the double mutant discussed above, and (ii) replacing Asp with Ala, which will remove the side chain and hence alter the dynamics.

The large decrease in $k_{AB}^{(2)}$ in the double mutant compared to the single mutants shows a cooperative effect of these two Asp residues for proton transfer through the proton-transfer pathway as indicated in Figure 6.

(B) Uptake of the Second Proton [H$^+$(2)] during $k_{AB}^{(1)}$. The changes in $k_{AB}^{(1)}$ in the double mutant [DN(L210)/DN-(M17)] also suggest changes in the rate of proton transfer of H$^+$(2) to Glu-L212; however, the evidence is not as conclusive as for $k_{AB}^{(2)}$ discussed above. The coupling between proton binding and electron transfer for $k_{AB}^{(1)}$ occurs mainly at pH $\geq$8, where the protonation of Glu-L212, located near Q_B, accompanies electron transfer (see eq 1). This conclusion is based on the observation that in Glu-L212 $\rightarrow$ Gln mutant RCs, $k_{AB}^{(1)}$ is pH-independent and has the same value as in native RCs at pH <7 (*7, 9*). Subsequent calculations have corroborated that conclusion (*32*). In native RCs at pH >8, when Glu-L212 is deprotonated prior to electron transfer, $k_{AB}^{(1)}$ decreases with increasing pH (*7, 9, 24*). At lower pH (pH <7), the electron transfer is gated by a conformational step that could involve the movement or reorientation of water molecules or nearby polar groups or internal proton rearrangements (*15, 25, 29, 32*−*34*).

To confirm that in the double mutant RCs the measured rates probe the protonation of Glu-L212 at pH 8, as has been shown for native RCs (*7, 9*), a triple mutant lacking Asp-L210, Asp-M17, and Glu-L212 [i.e., DN(L210)/EQ(L212)/DN(M17)] was constructed, and the electron-transfer and proton uptake rates were measured. In the triple mutant RCs, $k_{AB}^{(1)}$ has nearly the same value as in native RCs (pH < 8) and is pH independent (data not shown). In addition, the amplitude of the associated proton uptake is decreased by an order of magnitude. These observations support previous proposals that the majority of proton uptake at pH $\geq$8 is associated with protonation of Glu-L212 (*9, 35, 36*).

The requirement that Glu-L212 be protonated for favorable electron transfer explains the reduction of $k_{AB}^{(1)}$ at pH > pK_a of Glu-L212 (Figure 2). In native RCs, the observed decrease in $k_{AB}^{(1)}$ is consistent with a p$K_a^{obs} \sim$ 8.5 for Glu-L212 (*7, 9*). For the single mutant RCs, DN(L210) and DN-(M17), the slower rates ($\sim$8-fold, pH 8) (Table 1) can be attributed to a shift in the pK_a of Glu-L212 to lower pH as expected from the loss of a negative charge interacting with Glu-L212. In the double mutant RCs, the value for $k_{AB}^{(1)}$ can, in principle, be explained by either (i) a larger change in the pK_a of Glu-L212 than in the single mutants or (ii) a decrease in the rate of transfer of H$^+$(1) if proton transfer were rate-limiting. Evidence that the change in $k_{AB}^{(1)}$ in the double mutant is due to a rate-limiting proton transfer is indicated by the change in the pH dependence of $k_{AB}^{(1)}$ (Figure 2). The difference in slope suggests that the rate-limiting step is different in the double mutant compared to native or single mutant RCs. Evidence that there is no larger pK_a shift in the double mutant than in the single mutants is provided by the similarity of k_{BD} to that of the single mutant RCs (data not shown). A large change in the protonation state of Glu-L212 would be expected to produce large changes in k_{BD} due to electrostatic destabilization of $Q_B^{-\bullet}$ by the ionization of Glu-L212. Thus, the small value for $k_{AB}^{(1)}$ observed in the double mutant RCs is attributed to a reduction in the rate of proton transfer of H$^+$(1) due to the simultaneous replacement of Asp-L210 and Asp-M17 with Asn.

The properties of $k_{AB}^{(1)}$ and proton uptake in the double mutant are similar to those observed in native RCs upon binding of one of the proton-transfer inhibitors (Zn^{2+}, Cd^{2+}, Ni^{2+}), in which the rate of protonation of Glu-L212 was inhibited (*25*). We, therefore, propose that the slow rate of $k_{AB}^{(1)}$ in the double mutant is a consequence of a slow rate-limiting protonation of Glu-L212.

The Cooperative Effect of Asp-L210 and Asp-M17 on the Rate of Proton Transfer. Although the role of Asp-L210 and Asp-M17 in providing parallel branches for proton transfer is clearly shown by the results discussed above, the question that remains to be answered is whether there exists a cooperative effect between them. For the case of two equivalent noninteracting pathways, the proton-transfer rate would be twice that for the individual pathways. Although the intrinsic proton-transfer rates in native and mutant RCs are not all known, experiments performed in the presence of a bound Cd^{2+}, which makes proton transfer the rate-limiting step of $k_{AB}^{(2)}$, show that the proton-transfer rate through the physiological pathways in native RCs with both Asp active is more than 10-fold greater than in the single mutant RCs with only one Asp active (*16*). Thus, there is a cooperative effect of Asp-L210 and Asp-M17 on the proton-transfer rate.

The observed cooperativity can be explained by the close proximity of the two acidic groups and nearby water molecules, resulting in a large electrostatic interaction between them (*31*). This interaction will favor the binding of a proton by either of the pair of acidic groups or a nearby water molecule, making it a better proton acceptor than it would be in the absence of the interaction. The magnitude of the interaction can be estimated from Coulomb's Law. For a distance of $\sim$5 Å, the distance between the two carboxylates (Figure 6), and a dielectric constant of 10, the electrostatic interaction is $\sim$290 meV. This interaction would result in raising the pK_a of one group by the presence of the other by nearly 5 pH units. One possible mechanism for the cooperative effect on proton transfer of Asp-M17 and Asp-L210 involves an electrostatic switch. Let us consider a simple example. The large electrostatic interactions among the carboxylic acid groups in the vicinity of Asp-L210 raise its pK_a. It has been estimated from continuum electrostatic calculations that the pK_a of Asp-L210 is above pH 8 (*32*). Protonation (neutralization) of Asp-M17 would eliminate its electrostatic interaction with Asp-L210, thereby lowering the pK_a of Asp-L210 (by as much as 5 pH units, see above), making it a better proton donor to $Q_B^{-\bullet}$. Thus, the protonation of Asp-M17 could induce proton transfer from Asp-L210 to $Q_B^{-\bullet}$. Although other mechanisms can be envisaged, the switching mechanism has the advantage of involving two different steps that can be independently optimized; i.e., Asp-M17 can be optimized for protonation from His-H126, while the protonated Asp-L210 can be independently optimized for proton transfer to $Q_B^{-\bullet}$.

The key component of the cooperative mechanism discussed above is the electrostatic interaction between Asp-L210 and Asp-M17. To investigate its importance for efficient proton transfer, we are constructing mutations to Lys, Arg, and His at each site.

The Involvement of Asp-L213 in the Proton-Transfer Pathway in Rb. sphaeroides. The similarity between the characteristics of $k_{AB}^{(1)}$ and $k_{AB}^{(2)}$ reported in this work in the double mutant RCs and those previously reported in the Asp-L213 → Asn mutant RCs (*8*−*10*, *20*, *34*) suggests that the physiological proton-transfer pathway is blocked both in the Asp-L213 → Asn and in the double mutant RCs. Therefore, the physiological pathways for $H^+(1)$ and $H^+(2)$ share the involvement of Asp-L213, as previously proposed (*9*, *10*, *37*). Thus, Asp-L213 provides a branch point from which $H^+(1)$ proceeds to $Q_B^{-\bullet}$ via Ser-L223 (*38*) and $H^+(2)$ proceeds to Glu-L212 via water molecules (see Figure 6).

The Dominant Proton-Transfer Pathways in RCs of Rb. sphaeroides. We have previously located the entry point for both protons [$H^+(1)$ and $H^+(2)$] associated with the reduction of Q_B to Q_BH_2 (eqs 1−3) at the surface-accessible region on the H-subunit (His-H126, His-H128, and Asp-H124) (*15*). This conclusion was based on the location of the proton-transfer inhibitors Zn^{2+}, Cd^{2+}, and Ni^{2+} (*14*, *16*, *25*). In this work, we address the question of the proton-transfer pathway connecting the entry point with the $Q_B^{-\bullet}$ site.

Located in the intervening region between the entry point and $Q_B^{-\bullet}$ are Asp-L210 and Asp-M17 (Figure 6). Upon replacement of Asp-L210 or Asp-M17 with Asn, the rate of proton transfer, previously measured in RCs with a bound Cd^{2+}, was ∼10-fold slower (pH 8) than in native RCs (*16*). This showed the importance of Asp-L210 and Asp-M17 for efficient proton transfer. However, in the absence of the bound Cd^{2+}, the single mutant RCs showed essentially no change in $k_{AB}^{(2)}$ (Figure 4). Since in this case proton transfer is not rate-limiting, a reduction in the proton-transfer rate is not reflected in the observed rate (*16*). Thus, neither Asp-L210 nor Asp-M17 are by themselves crucial for RC function. The simplest interpretation of these results is that Asp-L210 and Asp-M17 provide two possible, parallel, branches for proton transfer from the RC surface to $Q_B^{-\bullet}$.

The results discussed in the previous sections show that the rates of proton transfer of $H^+(1)$ (eq 2) and $H^+(2)$ (eq 1) are drastically slowed ($\geq 10^3$-fold) in the double mutant. These results provide independent evidence for the proton-transfer pathways that were previously proposed based on the inhibition of proton transfer by the binding of divalent metal ions (*14*−*16*, *25*). The physiologically active pathways for the transfer of $H^+(1)$ and $H^+(2)$ share, in addition to the entry point (*25*), the involvement of Asp-L210 and Asp-M17 as shown in Figure 6.

The uptake and transfer of the proton from the solvent, the ultimate source of the protons, to $Q_B^{-\bullet}$ can occur in several independent steps (see Figure 6): (1) Proton uptake from the solvent by His-H126 and/or His-H128. The involvement of the His side chains in the proton-transfer pathway was shown by the decreased $k_{AB}^{(1)}$ and $k_{AB}^{(2)}$ values in RCs in which both His were replaced with Ala (*39*). (2) Proton transfer from His-H126 and/or His-H128 to Asp-L210 and/or Asp-M17, the involvement of which has been discussed above. (3) Proton transfer from Asp-L210/Asp-M17 to Asp-L213 (see discussion above). (4) For $H^+(1)$, proton transfer from Asp-L213 to $Q_B^{-\bullet}$ via Ser-L223 (*38*); for $H^+(2)$, proton transfer from Asp-L213 to Glu-L212 via water molecules. Upon $Q_B^{-\bullet}$ formation, the water molecules that bridge the gap between Asp-L213 and Glu-L212 are displaced (*29*). Thus, the structure supports the idea that protonation of Glu-L212 is required prior to $Q_B^{-\bullet}$ formation, which is suggested by the kinetic analysis and electrostatic calculations (*25*, *32*, *40*). Subsequently, $H^+(2)$ is transferred from the protonated Glu-L212 to Q_BH^- (see eq 3). Having identified the different proton-transfer steps, the remaining task is to determine the sequential order of the transfer events and the rates of the individual steps.

Proton Transfer through Other Crystallographically Resolved Putative Proton-Transfer Pathways in Rb. sphaeroides. From an analysis of the X-ray crystal structure of the RC, several possible pathways for proton transfer to reduced Q_B had been proposed. These include a long chain of water molecules connecting the region near Glu-L212 to the surface of the H subunit near Asp-M240 (*11*, *41*, *42*) and a pathway which includes a pool of water molecules connecting Asp-L213 to the RC surface near Tyr-M3, which is located near the proposed membrane−water interface (*28*, *42*). The proton-transfer rate through these putative pathways cannot be larger than the residual rate of $\sim 4\ s^{-1}$ that is observed in the double mutant RCs. This makes these pathways $\sim 10^3$-fold less effective than the pathway discussed above (Figure 6), since the rate of proton transfer in native RCs is $\geq 10^4\ s^{-1}$ (see above). This shows that the other postulated pathways, including the one composed of a continuous chain of water molecules, are not effective for proton transfer in the native bacterial RC from *Rb. sphaeroides*. On this basis, we favor the view that proton transfer occurs through a specific, optimized, proton-transfer pathway rather than diffuse delocalized pathways as has been suggested (*43*).

Proton Transfer in Other Photosynthetic Bacteria. The pathway discussed in this paper was determined for *Rb. sphaeroides*. Given the sequence homology with *Rb. capsulatus* (*44*, *45*), a similar proton-transfer pathway in that species is likely. It is noteworthy that even in the RC from the distantly related bacterium *Themochromatium tepidum*, there exists a coupled carboxylic acid pair (Asp-H124, Asp-M235) located near a pair of His (His-H122, His-M239) and the Q_B region (*46*). The similarities between the local structures of these distantly related species suggest the evolution of a common motif for the proton-transfer pathways.

Common Motifs of Proton Transfer in Other Systems. The physiological proton-transfer pathways identified in the bacterial RC (Figure 6) share some common characteristics with pathways elucidated in other systems. Proton conduction has been noted to be inhibited by certain metal ions (e.g., Zn^{2+} or Cd^{2+}). A blockage of activity by binding of Zn^{2+}, similar to that observed in the bacterial RC (*14*, *47*), has been reported in the ubiquinol:cytochrome *c* oxidoreductases (*48*), terminal oxidases (*49*), and voltage-gated proton channels (see, e.g., *50*). It has been suggested, based on proton pulse measurements made in cytochrome oxidase, that His residues could form part of a "proton collecting antenna" which facilitates proton entry into the protein (*51*).

As in RCs, there is also an involvement of carboxylic acids in the proton-transfer pathways of many proteins involved in bioenergetics. The carboxylates can serve as proton donors/acceptors that electrostatically stabilize the proton in the interior of the protein (see, e.g., *52*). The involvement of carboxylic acid groups in proton conduction has also been suggested in bacteriorhodopsin (reviewed in *53*, *54*), terminal oxidases (reviewed in *55*, *56*), lac permease (reviewed in

57), ubiquinol:cytochrome *c* oxidoreductases (*58*−*60*), NADH: ubiquinone oxidoreductase (*61*), and fumarate reductase (*62*). Thus, the involvement of carboxylic acid residues represents a general strategy used to lower the electrostatic barrier to proton conduction through proteins.

ACKNOWLEDGMENT

We thank Herbert Axelrod for helpful discussions.

NOTE ADDED IN PROOF

We have recently replaced each of the Asp-L210 and Asp-M17 with Lys to investigate the effect on proton transfer due to the increase in the electrostatic barrier (charge change of +2) near the proton entry point (Figure 6). In both mutants $k_{AB}^{(2)}$ decreased ∼30-fold compared to native RCs showing that the introduction of the positive Lys residue electrostatically destabilizes proton binding/transfer along the chain. However, the observed rate is ∼10-fold greater than in the double mutant [DN(L210)/DN(M17)] (see Table 1). A simple explanation of the greater value of $k_{AB}^{(2)}$ in these single mutants, compared to the double mutant, is that the carboxylate of the unmutated Asp can act as a proton transfer component. Thus, these results are consistent with the idea that Asp-L210 and Asp-M17 are important for their function as components of the proton transfer chain as well as their ability to stabilize protons in the interior of the protein.

REFERENCES

1. Feher, G., Allen, J. P., Okamura, M. Y., and Rees, D. C. (1989) *Nature 339*, 111−116.
2. Blankenship, R. E., Madigan, M. T., and Bauer, C. E., Eds. (1995) *Anoxygenic Photosynthetic Bacteria*, Kluwer Academic Publishers, Dordrecht, The Netherlands.
3. Graige, M. S., Paddock, M. L., Bruce, J. M., Feher, G., and Okamura, M. Y. (1996) *J. Am. Chem. Soc. 118*, 9005−9016.
4. Crofts, A. R., and Wraight, C. A. (1983) *Biochim. Biophys. Acta 726*, 149−185.
5. McPherson, P. H., Okamura, M. Y., and Feher, G. (1990) *Biochim. Biophys. Acta 1016*, 289−292.
6. Gunner, M. (1991) *Curr. Top. Bioenerg. 16*, 319−367.
7. Paddock, M. L., Rongey, S. H., Feher, G., and Okamura, M. Y. (1989) *Proc. Natl. Acad. Sci. U.S.A. 86*, 6602−6606.
8. Takahashi, E., and Wraight, C. A. (1990) *Biochim. Biophys. Acta 1020*, 107−111.
9. Takahashi, E., and Wraight, C. A. (1992) *Biochemistry 31*, 855−866.
10. Paddock, M. L., Rongey, S. H., McPherson, P. H., Juth, A., Feher, G., and Okamura, M. Y. (1994) *Biochemistry 33*, 734−745.
11. Baciou, L., and Michel, H. (1995) *Biochemistry 34*, 7967−7972.
12. Takahashi, E., and Wraight, C. A. (1996) *Proc. Natl. Acad. Sci. U.S.A. 93*, 2640−2645.
13. Okamura, M. Y., Paddock, M. L., Graige, M. S., and Feher, G. (2000) *Biochim. Biophys. Acta 1458*, 148−163.
14. Paddock, M. L., Graige, M. S., Feher, G., and Okamura, M. Y. (1999) *Proc. Natl. Acad. Sci. U.S.A. 96*, 6183−6188.
15. Axelrod, H. L., Abresch, E. C., Paddock, M. L., Okamura, M. Y., and Feher, G. (2000) *Proc. Natl. Acad. Sci. U.S.A. 97*, 1542−1547.
16. Paddock, M. L., Feher, G., and Okamura, M. Y. (2000) *Proc. Natl. Acad. Sci. U.S.A. 97*, 1548−1553.
17. Paddock, M. L., Chang, C., Abresch, E. C., Feher, G., and Okamura, M. Y. (2001) *Biophys. J. 80*, 28A.
18. Lin, X., Williams, J. C., Allen, J. P., and Mathis, P. (1994) *Biochemistry 33*, 13517−13523.
19. Isaacson, R. A., Lendzian, F., Abresch, E. C., Lubitz, W., and Feher, G. (1995) *Biophys. J. 69*, 311−322.
20. Paddock, M. L., Senft, M. E., Graige, M. S., Rongey, S. H., Turanchik, T., Feher, G., and Okamura, M. Y. (1998) *Photosynth. Res. 55*, 281−291.
21. Kleinfeld, D., Okamura, M. Y., and Feher, G. (1984) *Biochim. Biophys. Acta 766*, 126−140.
22. Labahn, A., Bruce, J. M., Okamura, M. Y., and Feher, G. (1995) *Chem. Phys. 197*, 355−366.
23. Vermeglio, A., and Clayton, R. K. (1977) *Biochim. Biophys. Acta 461*, 159−165.
24. Kleinfeld, D., Okamura, M. Y., and Feher, G. (1985) *Biochim. Biophys. Acta 809*, 291−310.
25. Ädelroth, P., Paddock, M. L., Sagle, L. B., Feher, G., and Okamura, M. Y. (2000) *Proc. Natl. Acad. Sci. U.S.A. 97*, 13086−13091.
26. Nabedryk, E., Breton, J., Okamura, M. Y., and Paddock, M. P. (2001) *Biophys. J. 80*, 427−428A.
27. Sebban, P., Maróti, P., Schiffer, M., and Hanson, D. K. (1995) *Biochemistry 34*, 8390−8397.
28. Paddock, M. L., Axelrod, H. L., Abresch, E. C., Yeh, A. P., Rees, D. C., Feher, G., and Okamura, M. Y. (1999) *Biophys. J. 76*, 141A.
29. Stowell, M. H. B., McPhillips, T. M., Rees, D. C., Soltis, S. M., Abresch, E., and Feher, G. (1997) *Science 276*, 812−816.
30. Kraulis, P. J. (1991) *J. Appl. Crystallogr. 24*, 946−950.
31. Merritt, E. A., and Bacon, J. D. (1997) *Methods Enzymol. 277*, 505−524.
32. Alexov, E. G., and Gunner, M. R. (1999) *Biochemistry 38*, 8253−8270.
33. Tiede, D. M., Vazquez, J., Cordova, J., and Marone, P. A. (1996) *Biochemistry 35*, 10763−10775.
34. Graige, M. S., Feher, G., and Okamura, M. Y. (1998) *Proc. Natl. Acad. Sci. U.S.A. 95*, 11679−11684.
35. McPherson, P. H., Schönfeld, M., Paddock, M. L., Okamura, M. Y., and Feher, G. (1994) *Biochemistry 33*, 1181−1193.
36. Miksovska, J., Maróti, P., Tandori, J., Schiffer, M., Hanson, D. K., and Sebban, P. (1996) *Biochemistry 35*, 15411−15417.
37. McPherson, P. H., Rongey, S. H., Paddock, M. L., Feher, G., and Okamura, M. Y. (1991) *Biophys. J. 59*, 142A
38. Paddock, M. L., McPherson, P. H., Feher, G., and Okamura, M. Y. (1990) *Proc. Natl. Acad. Sci. U.S.A. 87*, 6803−6807.
39. Ädelroth, P., Paddock, M. L., Beatty, J. T., Feher, G., and Okamura, M. Y. (2001) *Biophys. J. 80*, 427A.
40. Grafton, A. K., and Wheeler, R. A. (1999) *J. Phys. Chem. 103*, 5380−5387.
41. Ermler, U., Fritzsch, G., Buchanan, S. K., and Michel, H. (1994) *Structure 2*, 925−936.
42. Abresch, E. C., Paddock, M. L., Stowell, M. H. B., McPhillips, T. M., Axelrod, H. L., Soltis, S. M., Rees, D. C., Okamura, M. Y., and Feher, G. (1998) *Photosynth. Res. 55*, 119−125.
43. Gerencsér, L., and Maróti, P. (2001) *Biochemistry 40*, 1850−1860.
44. Williams, J. C., Steiner, L. A., Feher, G., and Simon, M. I. (1984) *Proc. Natl. Acad. Sci. U.S.A. 81*, 7303−7307.
45. Youvan, D. C., Bylina, E. J., Alberti, M., Begusch, H., and Hearst, J. E. (1984) *Cell 37*, 949−957.
46. Nogi, T., Fathir, I., Kobayashi, M., Nozawa, T., and Miki, K. (2000) *Proc. Natl. Acad. Sci. U.S.A. 97*, 13561−13566.
47. Utschig, L. M., Ohigashi, Y., Thurnauer, M. C., and Tiede, D. M. (1998) *Biochemistry 37*, 8278−8281.
48. Link, T. A., and von Jagow, G. (1995) *J. Biol. Chem. 270*, 25001−25006.
49. Aagaard, A., and Brzezinski, P. (2001) *Biophys. J. 80*, 190A.
50. DeCoursey, T. E., and Cherney, V. V. (2000) *Biochim. Biophys. Acta 1458*, 104−119.
51. Marantz, Y., Nachliel, E., Aagaard, A., Brzezinski, P., and Gutman, M. (1998) *Proc. Natl. Acad. Sci. U.S.A. 95*, 8590−8595.
52. Gutman, M., and Nachliel, E. (1995) *Biochim. Biophys. Acta 1231*, 123−138.
53. Lanyi, J. K. (1998) *J. Struct. Biol. 124*, 164−178.
54. Haupts, U., Tittor, J., and Oesterhelt, D. (1999) *Annu. Rev. Biophys. Biomol. Struct. 28*, 367−399.

55. Brzezinski, P., and Ädelroth, P. (1998) *J. Bioenerg. Biomembr. 30*, 99−107.
56. Mills, D. A., and Ferguson-Miller, S. (1998) *Biochim. Biophys. Acta 1365*, 46−52.
57. Kaback, H. R., and Wu, J. H. (1997) *Q. Rev. Biophys. 30*, 333−364.
58. Gennis, R. B., Barquera, B., Hacker, B., Van Doren, S. R., Arnaud, S., Crofts, A. R., Davidson, E., Gray, K. A., and Daldal, F. (1993) *J. Bioenerg. Biomembr. 25*, 195−209.
59. Zito, F., Finazzi, G., Joliot, P., and Wollman, F.-A (1998) *Biochemistry 37*, 10395−10403.
60. Crofts, A. R., Hong, S. J., Ugulava, N., Barquera, B., Gennis, R., Guergova-Kuras, M., and Berry, E. A. (1999) *Proc. Natl. Acad. Sci. U.S.A. 96*, 10021−10026.
61. Hellwig, P., Scheide, D., Bungert, S., Mäntele, W., and Friedrich, T. (2000) *Biochemistry 39*, 10884−10891.
62. Lancaster, C. R. D., Gross, R., Haas, A., Ritter, M., Mäntele, W., Simon, J., and Kröger, A. (2000) *Proc. Natl. Acad. Sci. U.S.A. 97*, 13051−13056.

BI010280A